

Research Article: New Research / Development

NMNAT proteins that limit Wallerian degeneration also regulate critical period plasticity in the visual cortex

Mariska van Lier¹, Laura Smit-Rigter¹, Roos Krimpenfort¹, M. Hadi Saiepour¹, Emma Ruimschotel¹, Willem Kamphuis³, J. Alexander Heimerl² and Christiaan N. Levelt^{1,4}

¹*Molecular Visual Plasticity Group, Netherlands Institute for Neuroscience, Meibergdreef 47, 1105 BA Amsterdam, the Netherlands*

²*Cortical Structure and Function Group, Netherlands Institute for Neuroscience, Meibergdreef 47, 1105 BA Amsterdam, the Netherlands*

³*Netherlands Institute for Neuroscience, Meibergdreef 47, 1105 BA Amsterdam, the Netherlands*

⁴*Department of Molecular and Cellular Neurobiology, Center for Neurogenomics and Cognitive Research, VU University Amsterdam, de Boelelaan 1085, 1081 HV, the Netherlands.*

<https://doi.org/10.1523/ENEURO.0277-18.2018>

Received: 17 July 2018

Revised: 3 December 2018

Accepted: 4 December 2018

Published: 4 January 2019

Author Contributions:

MVL, LSR, JAH and CNL designed research, MVL, LSR, RK, MHS, ER, WK and JAH performed research, MVL, LSR, RK, WK and JAH analyzed data, MVL and CNL wrote the paper.

Funding: AgentschapNL NeuroBasic PharmaPhenomics

Funding: NWO
823.02.001
Vidi

Funding: Stichting Blindenhulp

Funding: Praktijkgenerator b.v.

Conflict of Interest: Authors report no conflict of interest

Funding sources:

This work was funded through a grant from AgentschapNL to the NeuroBasic PharmaPhenomics consortium (CNL), NWO grant 823.02.001 to CNL, a grant from Stichting Blindenhulp, a donation from Praktijkgenerator b.v. and a Vidi grant to JAH.

M.V.L. and L.S.R. these authors contributed equally.

Correspondence should be addressed to: Christiaan N. Levelt, c.levelt@nin.knaw.nl

Cite as: eNeuro 2019; 10.1523/ENEURO.0277-18.2018

Alerts: Sign up at www.eneuro.org/alerts to receive customized email alerts when the fully formatted version of this article is published.

Accepted manuscripts are peer-reviewed but have not been through the copyediting, formatting, or proofreading process.

Copyright © 2019 van Lier et al.

This is an open-access article distributed under the terms of the Creative Commons Attribution 4.0 International license, which permits unrestricted use, distribution and reproduction in any medium provided that the original work is properly attributed.

1 **1. Manuscript Title:**

2 **NMNAT proteins that limit Wallerian degeneration also regulate critical period plasticity**
3 **in the visual cortex**

4

5 **2 Abbreviated Title:**

6 **Regulation of critical period plasticity by NMNAT**

7

8 **3. Authors:**

9 Mariska van Lier^{1*}, Laura Smit-Rigter^{1*}, Roos Krimpenfort¹, M. Hadi Saiepour¹, Emma
10 Ruimschotel¹, Willem Kamphuis³, J. Alexander Heimel² and Christiaan N. Levelt^{1,4}

11 ¹Molecular Visual Plasticity Group, Netherlands Institute for Neuroscience, Meibergdreef 47,
12 1105 BA Amsterdam, the Netherlands

13 ²Cortical Structure and Function Group, Netherlands Institute for Neuroscience, Meibergdreef
14 47, 1105 BA Amsterdam, the Netherlands

15 ³Netherlands Institute for Neuroscience, Meibergdreef 47, 1105 BA Amsterdam

16 ⁴Department of Molecular and Cellular Neurobiology, Center for Neurogenomics and Cognitive
17 Research, VU University Amsterdam, de Boelelaan 1085, 1081 HV, the Netherlands.

18 *these authors contributed equally.

19

20 **4. Author Contributions:**

21 MVL, LSR, JAH and CNL designed research, MVL, LSR, RK, MHS, ER, WK and JAH

22 performed research, MVL, LSR, RK, WK and JAH analyzed data, MVL and CNL wrote the

23 paper.

24

25 **5. Correspondence should be addressed to:**

26 CNL c.levelt@nin.knaw.nl, +31-20-5665359

27 **Number of Figures: 6**

28 **Number of Tables: 0**

29 **Number of Multimedia: 0**

30 **Number of words for Abstract: 203**

31 **Number of words for Significance Statement: 67**

32 **Number of words for Introduction: 766**

33 **Number of words for Discussion: 788**

34

35 **Acknowledgements:**

36 The authors like to thank Toshiyuki Araki for donating the NMNAT1 and NMNAT3 transgenic
37 mice.

38

39 **Authors report no conflict of interest**

40

41 **Funding sources:**

42 This work was funded through a grant from AgentschapNL to the NeuroBasic

43 PharmaPhenomics consortium (CNL), NWO grant 823.02.001 to CNL, a grant from Stichting

44 Blindenhulp, a donation from Praktijkgenerator b.v. and a Vidi grant to JAH.

45

46 **Abstract**

47 Many brain regions go through critical periods of development during which plasticity is
48 enhanced. These critical periods are associated with extensive growth and retraction of
49 thalamocortical and intracortical axons. Here, we investigated whether a signaling pathway that
50 is central in Wallerian axon degeneration also regulates critical period plasticity in the primary
51 visual cortex. Wallerian degeneration is characterized by rapid disintegration of axons once they
52 are separated from the cell body. This degenerative process is initiated by reduced presence of
53 cytoplasmic nicotinamide mononucleotide adenylyltransferases (NMNATs) and is strongly
54 delayed in mice overexpressing cytoplasmic NMNAT proteins, such as *Wld^S* mutant mice
55 producing a UBE4b-NMNAT1 fusion protein or NMNAT3 transgenic mice. Here we provide
56 evidence that in *Wld^S* mice and NMNAT3-transgenic mice, ocular dominance plasticity in the
57 developing visual cortex is reduced. This deficit is only observed during the second half of the
58 critical period. Additionally, we detect an early increase of visual acuity in the primary visual
59 cortex of *Wld^S* mice. We do not find evidence for Wallerian degeneration occurring during ocular
60 dominance plasticity. Our findings suggest that NMNATs do not only regulate Wallerian
61 degeneration during pathological conditions, but also control cellular events that mediate critical
62 period plasticity during the physiological development of the cortex.

63

64 **Significance statement**

65 Different forms of axon degeneration occur during development and neurodegenerative
66 processes. A good understanding of the molecular and cellular events that regulate these forms
67 of axon degeneration is essential to selectively modulate them for therapeutic purposes. This
68 study shows that genes thought to be selectively involved in pathological axon degeneration are
69 also involved in developmental plasticity, implying that these events are molecularly less
70 separable than previously assumed.

71

72 Introduction

73 Many regions of the brain go through defined phases of development, known as critical periods,
74 during which experience-dependent plasticity is enhanced. Plasticity deficits during these critical
75 periods have lifelong consequences. Understanding the molecular and cellular mechanisms
76 that control critical period closure may help the development of approaches to reopen critical
77 periods at a later age for therapeutic purposes. The most informative model to study critical
78 period regulation has been ocular dominance (OD) plasticity in mouse primary visual cortex
79 (V1). OD plasticity occurs during development in order to optimize binocular vision, matching
80 the inputs of both eyes and, if this is not possible, biasing V1 towards inputs from the eye
81 providing the most reliable inputs. When one eye is monocularly deprived (MD) for several days,
82 developing V1 adjusts to this situation by rearranging thalamocortical and corticocortical
83 connectivity. This results in a shift of responsiveness of V1 neurons towards the open eye
84 (Antonini et al., 1999; Gordon and Stryker, 1996; Haruta and Hata, 2007). In adult mice in which
85 the critical period in V1 is closed, prolonged MD causes a weaker and less permanent shift
86 (Heimel et al., 2007; Hofer et al., 2006; Lehmann and Löwel, 2008; Sato and Stryker, 2008;
87 Sawtell et al., 2003). Over the last two decades, this model revealed that maturation of inhibitory
88 innervation is the dominant mechanism regulating critical period closure. However, various other
89 cellular events have been implicated in critical period closure, including excitatory synapse
90 maturation (Bochner et al., 2014; Huang et al., 2015; Jenks et al., 2017; Stephany et al., 2014;
91 Tropea et al., 2010), extracellular matrix development (Pizzorusso et al., 2002), CREB-
92 transcription (Pham et al., 2004; Tognini et al., 2011), neuromodulatory inputs (Bear and Singer,
93 1986; Morishita and Hensch, 2008; Vetencourt et al., 2008) and declining neurite growth and
94 retraction (McGee et al., 2005; Syken et al., 2006).

95 In a study analyzing changes in the synaptic proteome during development and OD plasticity of
96 V1 several proteins involved in Wallerian axon degeneration were identified, whose expression
97 levels changed around the time of critical period closure (Dahlhaus et al., 2011). Wallerian
98 degeneration typically occurs after the nerve is separated from the cell body after injury
99 (Coleman and Freeman, 2010; Geden and Deshmukh, 2016; Gerdts et al., 2016;
100 Kerschensteiner et al., 2005; Pease and Segal, 2014). Because retraction of thalamocortical
101 and intracortical axons also occurs in V1 during OD plasticity, we were intrigued by the
102 possibility that the signaling pathway that mediates Wallerian degeneration also regulates
103 axonal reorganization during OD plasticity.

104 During Wallerian degeneration, disintegration of the axon starts by breakdown of the
105 cytoskeleton, followed by degradation of the myelin sheath (Gilley and Coleman, 2010; Vargas
106 and Barres, 2007). Nicotinamide mononucleotide adenylyltransferases (NMNATs), key proteins
107 in the nicotinamide adenine dinucleotide (NAD) biosynthetic pathway, are implicated in
108 regulating Wallerian degeneration. Wallerian degeneration is slowed down considerably in *Wld^S*
109 mice, which carry a spontaneous mutation causing overexpression of an axonally targeted
110 UBE4b-NMNAT1 fusion protein (Coleman et al., 1998; Conforti et al., 2009, 2007, 2000; Lunn et
111 al., 1989; Lyon et al., 1993). NMNAT3, which is localized in mitochondria, can also protect
112 against Wallerian degeneration when overexpressed in transgenic mice (Yahata et al., 2009).
113 Interestingly, neither NMNAT1 nor NMNAT3, but NMNAT2 is required for axon integrity (Gilley

114 and Coleman, 2010). After axons are injured, NMNAT2 expression rapidly declines promoting
115 axon degeneration (Araki et al., 2004; Babetto et al., 2013; Sasaki et al., 2006).

116 Previous work found that axonal pruning during early development was not altered in *Wld^S* mice
117 and flies overexpressing the *Wld^S* protein (Hoopfer et al., 2006). This suggested that Wallerian
118 degeneration only occurs after injury and not during development. However, it has become clear
119 that early cortical development driven by spontaneous activity and critical period plasticity driven
120 by experience are regulated by different molecular and cellular mechanisms (Hensch, 2005;
121 Levelt and Hübener, 2012; Lohmann and Kessels, 2014). Therefore, we wanted to reassess the
122 premise that the Wallerian degeneration signaling pathway is not involved in normal
123 development of the brain.

124 To this aim, we assessed whether OD plasticity is altered in mouse lines in which Wallerian
125 degeneration is reduced due to overexpression of cytoplasmic NMNAT overexpression. We find
126 that in mice overexpressing NMNAT in the cytoplasm, OD plasticity is reduced during the
127 second half of the critical period but not during the first half. Moreover, we find that cortical
128 visual acuity in *Wld^S* is already high at a young age. At the same time, we find that OD plasticity
129 does not cause hallmark signatures of Wallerian degeneration. Together, these results suggest
130 that genes that regulate Wallerian degeneration also regulate developmental events in the
131 visual cortex.

132

133

134 **Methods & Materials**

135 **Animals**

136 We made use of mice overexpressing the *Wld^S* protein, NMNAT1 (nuclear isoform) or NMNAT3
137 (mitochondrial isoform) (Yahata et al., 2009). The *Wld^S* line was originally derived from the
138 C57Bl/6Ola/hsd mouse line and hence, these mice were used as wildtype controls for these
139 mice. NMNAT1 and NMNAT3 mice were maintained on a C57Bl6/j background and wildtype
140 littermates were used as controls. Mice of either sex were used for all experiments. All
141 experiments involving mice were approved by the institutional animal care and use committee.

142 **Surgical preparation**

143 For monocular deprivation (MD), the upper and lower lids of the right eye were clipped and
144 sutured together with two mattress sutures during isoflurane anaesthesia. During the procedure
145 the eye was rinsed with saline and after suturing lidocaine cream was applied to the closed
146 eyelid. At the start of an imaging session, the eyes were re-opened. Animals which had early
147 opening of the eye or a damaged eye were excluded from the experiments.

148 **Optical imaging and visual stimulation**

149 Optical imaging of intrinsic signal was performed as previously described (Heimel et al., 2007).
150 Mice were anesthetized with an intraperitoneal injection of urethane (Sigma; 20% solution in
151 saline, 2 mg/10 g bodyweight). This was immediately followed by a subcutaneous injection of
152 atropine sulphate (AUV; 50 µg/mL in saline, 1 µg/10g bodyweight) to reduce excretions from
153 mucous membranes and chlorprothixene (Sigma; 2 mg/ml in saline, 80 µg/10g bodyweight).
154 Sometimes a supplement of urethane of about 10% of the initial dose was necessary to obtain a
155 sufficient amount of anaesthesia. Anesthetized mice were placed on a heating pad and body
156 temperature was monitored with a rectal probe and maintained at 36.5°C. A continuous flow of
157 oxygen was provided close to the nose. The mouse was fixated by ear bars with conical tips
158 and a bite rod behind the front teeth, 3 mm lower than the ear bars. The scalp was treated with
159 xylocaine (lidocaine HCL, AUV), and part of the scalp was removed to expose the skull. The
160 skull was cleaned using saline. Black cloth was used to prevent light from the monitor reaching
161 the camera. Light from a tungsten-halogen lamp filtered through a KG-1 heat filter and a 700 nm
162 (30 nm width) band-pass filter illuminated the skull. Reflecting light was caught by Adimec-
163 1000m/D CCD camera behind a macroscope composed of two Nikkor 50mm/f1.2 lenses,
164 focused 0.8 below the cranial surface, centred at 2.6 mm lateral and 0.5 rostral to lambda.
165 Images, taken at 25 Hz, were down sampled and stored 1.7 Hz by an Optimal Imager 3001
166 system (Optical Imaging Inc, Rehovot, Israel).

167 A gamma-corrected Dell UltraSharp U2312HM 23" full HD LCD monitor was placed at 15 cm
168 from the mouse' eye contralateral to the imaged hemisphere covering -15 to 75 degrees
169 horizontally and -45 to 45 degrees vertically of the visual field. Background luminance was 5 cd
170 m⁻². For obtaining a coarse retinotopic map, the screen was divided in two by two rectangles.
171 Square wave, 90% contrast, gratings of 0.05 cycles per degree drifting at 40 degrees per
172 second and changing drifting directions every 0.6 s, were intermittently shown for 6 s every 15 s
173 in one of the quadrants, on an equiluminant grey background, for about 15 repetitions. For
174 measuring ocular dominance, the same square wave gratings were shown in the superior-nasal
175 quadrant, for 3 s per stimulation. Using automated eye shutters, vision was allowed through the

176 left, the right or no eye (to check the completeness of the vision block) in random order (at least
177 40 repetitions for each condition). Acuity was measured by stimulating the contralateral eye with
178 sinusoidal, 90% contrast, gratings of various spatial frequencies, for at least 40 repetitions.
179 Visual stimuli were separated by periods of equiluminant grey of at least 12 s.

180 Image analysis was done by first subtracting signal average of the last 3 s before stimulation. To
181 remove global slow biological fluctuations, this signal was normalized by changes occurring in a
182 reference region outside of visual cortex. For each pixel, the response was computed as the
183 negative of this average signal during the visual stimulation. For retinotopic mapping, each pixel
184 received a colour corresponding to the quadrant to which the signal was highest. Using this
185 map, the area corresponding to the superior-nasal quadrant was manually selected as ROI for
186 the ocular dominance and acuity measurements. The response in these tests was taken as the
187 mean response over all pixels in this ROI. The imaged Ocular Dominance Index (iODI) was
188 defined as $(\text{contra response} - \text{ipsi response}) / (\text{contra response} + \text{ipsi response})$. The acuity
189 was defined by the intercept with the spatial frequency axis after fitting the spatial frequency
190 tuning curve with a downward sloping threshold linear function.

191 **Immunohistochemistry**

192 Age matched mice were anesthetized with 0.1 ml/g body weight Nembutal (Janssen) and
193 perfused with 4% paraformaldehyde (PFA) in PBS (~80 ml per mouse) and post-fixed for 2–3 h.
194 Coronal sections of 50 μm were made by using a vibratome (Leica VT1000S). Antibodies used
195 were against synaptotagmin-2 (rabbit, 1:1000, a kind gift from Dr. T. Südhof) followed by Alexa
196 Fluor 568-conjugated goat anti-rabbit antibody (1:000, A11011, Invitrogen) or the F4/80 marker
197 for activated microglia (mouse, 1:200, MCA497, BioRad) followed by Alexa Fluor 568-
198 conjugated goat anti-mouse antibody (1:500, A11004, Invitrogen). All antibodies were previously
199 tested in mice for the application we used them for (more information can be found in the
200 references or on the websites of the suppliers). Free-floating sections were briefly washed in
201 PBS followed by 1 h blocking in PBS containing 5% normal goat serum and 0.1% Triton X-100.
202 Primary antibody incubation was performed overnight at 4 °C in fresh blocking solution. Next,
203 the sections were washed three times for 10 min in PBS with 0.1% Tween-20 (PBST) followed
204 by secondary antibody incubation in fresh blocking solution for 90 min at RT. After washing
205 three times for 10 min in PBST the sections were mounted on glass slides using Mowiol
206 (Calbiochem/MerckMillipore) and glass covered for imaging.

207

208 **Confocal microscopy and data analysis**

209 For quantification of syt 2 puncta number, fluorescent puncta were analyzed using a non-
210 commercially available macro for Image-Pro PLUS (v6.3). Up to 6 puncta rings per image
211 obtained from V1 sections were manually encircled after which a mask was created on the cell.
212 A 2 μm wide ring was calculated around the mask and all puncta in the ring were considered to
213 belong to the cell and were counted and measured. Signals not reaching size and fluorescent
214 threshold levels were omitted. Pixel intensity for the signal within masks was considered
215 background and subtracted from the intensity values in the puncta. Puncta numbers were
216 analyzed per image. For quantification of the number of activated microglia, the number of
217 microglia cells were manually counted in images obtained from V1 sections. An area of 387.5
218 $\mu\text{m} \times 387.5 \mu\text{m}$ was counted. Only cells of which the soma was visible were included.

219 qPCR

220 RNA was isolated from tissue containing V1 from both control and Wld^S mice using the
221 *mirVana*TM miRNA isolation kit (Invitrogen). Total RNA (200 ng) was DNase I treated and used
222 as a template to generate cDNA following the manufacturer's instructions (QuantiTect Reverse
223 Transcription Kit-Qiagen) with a blend of oligo-dT and random primers. The reverse
224 transcriptase reaction was incubated at 42 °C for 30 min and terminated at 95 °C for 3 min. The
225 resulting cDNA was diluted 1:20 and served as a template in real-time qPCR assays (SYBR-
226 Green PCR Master Mix; Applied Biosystems). Primers were generated for *GAD65* and tested
227 for efficiency. The determined transcript levels of these target genes were normalized against
228 the levels of *GAPDH* determined in the same sample to control for variability in the amount and
229 quality of the RNA and the efficiency of the cDNA reaction.

230
231 Slice electrophysiology

232 Slice electrophysiology. Mice were anesthetized using isoflurane and then decapitated. Brains
233 were quickly removed and kept at 0°C in carbogenated (95% O₂ /5% CO₂) modified ACSF
234 containing choline chloride (110 mM choline chloride, 7 mM MgCl₂, 0.5 mM CaCl₂, 2.5 mM KCl,
235 11.6 mM Na-ascorbate, 3.10 mM Na-pyruvate, 1.25 mM NaH₂PO₄, 25 mM D-glucose, and 25
236 mM NaHCO₃), to prevent axon potentials in the brain during stressful conditions. 330 μm thick
237 coronal slices containing the visual cortex were cut on a vibratome (Microm HM650V; Thermo
238 Scientific) while keeping the slices in carbogenated modified ACSF (125 mM NaCl, 3 mM KCl, 2
239 mM MgSO₄, 2 mM CaCl₂, 10 mM glucose, 1.20 mM NaH₂PO₄ and 26 mM NaHCO₃) at 0°C.
240 After slicing, all slices were kept in ACSF at 35°C for 30-45 minutes for recovery, while
241 continuously bubbled with carbogen. Next, slices were kept in continuously carbogenated ACSF
242 at room temperature until use (1–6 h after slicing). To perform electrophysiological experiments,
243 slices were moved to a chamber with continuous in- and outflow of carbogenated ACSF at a
244 rate of 1-2 ml per minute at room temperature. For all experiments, a layer 2/3 pyramidal neuron
245 in the visual cortex was patched. A glass pipette with a resistance between 3 and 6 MΩ was
246 filled with intracellular solution containing 1mg/ml biocytin for post hoc staining of the patched
247 cell. After obtaining a gigaOhm seal, whole-cell patch clamp recordings were performed using
248 Axopatch 1D (Axon Instruments, Union City, California). When the cell was patched, several
249 currents were injected to see whether a cell was healthy and whether it showed a firing pattern
250 typical for a pyramidal neuron. Before recording mEPSCs, the bath solution was replaced with
251 ACSF containing 1μM TTX to block all voltage dependent sodium currents and 20 μM Gabazine
252 to block all GABA_A receptors. For all experiments, cells were clamped at -70 mV and mEPSCs
253 were measured during 5 minutes. Mini Analysis (Synaptosoft Inc.) was used for analyzing
254 mEPSCs. Recordings were included when the seal resistance bigger than > 1 GΩ, the series
255 resistance was smaller than 20 MΩ, the whole cell capacitance was smaller than 150 pF, the
256 resting potential was more negative than -60 mV and the RMS noise was less than 2.5 pA
257 (threshold cutoff in MiniAnalysis was set at 6, which is 2 to 2.5 times the value of the RMS
258 noise), before and after recording.

259
260 Western Blot

261 V1 from Wld^S and control mice, and the binocular part of V1 from control mice with or without
262 MD, were collected and homogenized in lysis buffer (LB) containing 150 mM sodium chloride,

263 1% Triton X-100, 50mM Tris pH 8, and a protease inhibitor cocktail (cOmplete™ Mini EDTA-
264 Free, Roche), using an electric homogenizer (IKA). Proteins were purified by centrifugation
265 (1000G) and the supernatant was collected. Protein content was measured by comparing with a
266 bovine serum albumin standard using a bicinchoninic acid (BCA) reaction kit (Thermo Fisher
267 Scientific/Pierce) and the optical density of the reagent was measured with an iEMS Reader MF
268 (Labsystems/Thermo Scientific). Western blotting was performed using the NuPAGE Novex Bis-
269 Tris pre-cast gel kit with a 4–12% gradient or the NuPAGE Novex Tris-acetate pre-cast gel kit
270 with a 3–8% gradient, in Invitrogen gel containers (Invitrogen). Gels were loaded with 60 µg
271 protein and run for 1 hour at 200 V (Bis-Tris gel) or 150 V (Tris-acetate gel). After separation
272 gels were transferred at 14 V overnight to PVDF Immobilon-FL transfer membranes (Millipore).
273 Protein membrane blots were stained with antibodies against synapsin 1 (rabbit, 1:250,
274 ab64581), synaptotagmin-2 (mouse, 1:250, znp-1, ZIRC), NMNAT2 (mouse, 1:50, B-10, Santa
275 Cruz Biotechnology), MYCBP2 (rabbit, 1:500, ab86078, Abcam) and GAPDH (mouse,
276 1:1000, MAB374, Merck), and analyzed using infrared secondary antibodies (LI-COR
277 Biosciences) and the Odyssey Infrared Imaging System (LI-COR). Imaged bands were
278 measured using the Odyssey application software and corrected for background intensities from
279 adjacent non-labeled lanes.

280

281 **Statistics**

282 We determined that the imaged OD index values were normally distributed using the Shapiro-
283 Wilk test. For testing differences in OD plasticity between transgenic and control mice, we
284 computed whether there was a significant interaction in a two-way ANOVA. For graphical
285 representation of significant differences between groups, we presented the results of post-hoc
286 Tukey–Kramer tests. Because puncta number and density, mEPSCs, western blot data and
287 *GAD65* mRNA levels were normally distributed (Shapiro-Wilk test), we used t-test when two
288 independent groups were compared.

289 Results

290 **Reduced OD plasticity in Wld^S mice**

291 We first set out to investigate whether the Wld^S mutation affects OD plasticity. To this end, we
292 used optical imaging of intrinsic signal to determine the OD in V1 of Wld^S mice and control
293 C57Bl/6Ola/hsd mice that were either monocularly deprived for 7 days during the peak of the
294 critical period (postnatal (P) days 28-35) or reared normally. We found that 7 days of MD
295 caused a stronger shift in OD in wildtype mice than in Wld^S mice (Fig. 1a, b). Thus, the Wld^S
296 mutation interferes with efficient critical period plasticity in V1.

297 **Unaffected plasticity and higher visual acuity in V1 of young Wld^S mice**

298 Axon degeneration involves the decreasing availability of NMNAT2 (Gilley and Coleman, 2010),
299 a process that is enhanced by the Phr1 E3 ubiquitin ligase MYCBP2 (Babetto et al., 2013).
300 Interestingly, MYCBP2 was found to down-regulate in V1 between P30 and P46 (Dahlhaus et
301 al., 2011). It is thus possible that this leads to a gradual increase of axon stability contributing to
302 declining plasticity. We therefore wanted to test whether the reduced plasticity observed in P28-
303 P35 Wld^S mice was not a plasticity deficit per se, but a selective decline of plasticity during the
304 later phase of the critical period. To this aim, we assessed whether at an earlier age, Wld^S mice
305 did show OD plasticity. We again used optical imaging of intrinsic signal to determine the OD in
306 Wld^S mice and control C57Bl/6Ola/hsd mice that were reared normally, or monocularly deprived
307 for 7 days, but now starting one week earlier (P20-P27). We found that 7 days of MD starting at
308 P20 induced a full OD shift in Wld^S mice, similar to what we observed in C57Bl/6Ola/hsd mice
309 (Fig. 1c, d). Therefore, we conclude that in Wld^S mice, OD plasticity is not deficient as such, but
310 is decreased during the second half of the critical period.

311 This finding suggested that other functional changes that normally occur around the end of the
312 critical period may also take place at a younger age in Wld^S mice. One such change is the
313 increase in cortical visual acuity from approximately 0.25 cpd at P25 to over 0.5 cpd at P35
314 (Gianfranceschi et al., 2003; Gordon and Stryker, 1996; Heimel et al., 2007; Huang et al., 1999).
315 We determined acuity in both Wld^S and control C57Bl/6Ola/hsd mice at P25, by making use of
316 optical imaging of intrinsic signal (Fig. 2a, b). It was previously shown that at this age, visual
317 acuity is still low in wildtype mice, but nearly at adult levels in mice overexpressing BDNF
318 causing premature cortical development (Huang et al., 1999). Similarly, we observed that at
319 P25, visual acuity in Wld^S mice was significantly higher than in control mice (0.4 vs 0.25 cpd,
320 Fig. 2c). Thus, acuity in V1 reaches high levels at a younger age in Wld^S mice than in control
321 mice.

322 **No evidence for altered inhibitory or excitatory synapse development in Wld^S mice**

323 In BDNF overexpressing mice, an early decline of OD plasticity and accelerated development of
324 visual acuity was associated with accelerated development of the GABAergic inhibitory system
325 (Hanover et al., 1999; Huang et al., 1999). One of the key players in the regulation of critical
326 periods are the parvalbumin expressing (PV+) basket cells (Chattopadhyaya, 2004; Fagiolini,
327 2004; Hensch, 2005; Kuhlman et al., 2013). The axon terminals of these PV+ neurons form
328 presynaptic boutons on the soma and proximal dendrites of their target neuron and the
329 development of the puncta-rings that they form coincides with the critical period (del Rio and de
330 Leca, 1994). We therefore set out to quantify the difference in perisomatic inhibition from PV+

331 interneurons onto pyramidal neurons in layer 2/3 and layer 5 of V1 in *Wld^S* mice and control
332 C57Bl/6Ola/hsd mice, by staining for synaptotagmin-2, a protein selectively expressed by PV+
333 boutons (Sommeijer and Levelt, 2012). Using immunohistochemistry and confocal microscopy,
334 we assessed the density of synaptotagmin-2 puncta at different developmental ages, P20 and
335 P30. However, we did not detect a difference in density of perisomatic synaptotagmin-2 puncta
336 in *Wld^S* mice compared to wildtype mice (Fig. 3a, b). Additionally, we studied whether there is
337 higher expression of synaptotagmin-2. Western blot analysis of V1 from P30 *Wld^S* and control
338 C57Bl/6Ola/hsd mice revealed no difference in synaptotagmin-2 levels (Fig. 3c). These findings
339 suggest that inhibitory innervation through PV+ interneurons is not responsible for the early
340 functional changes in V1 of *Wld^S* mice. To further investigate this, we studied the levels of the
341 glutamic acid decarboxylase GAD65, an enzyme involved in GABA synthesis. We used
342 quantitative PCR to determine levels of *Gad2* mRNA (encoding GAD65) relative to
343 housekeeping genes in V1 from P30 mice but found no difference between *Wld^S* and wildtype
344 control mice (Fig. 3d). Thus, our findings do not support the notion that development of
345 GABAergic innervation is accelerated in *Wld^S* mice.

346 Previous studies have shown that also excitatory synapse maturation affects critical period
347 onset and closure (Bochner et al., 2014; Huang et al., 2015; Jenks et al., 2017; Stephany et al.,
348 2014). We therefore studied whether excitatory synapses developed differently in *Wld^S* mice. In
349 order to determine this, we first quantified levels of the presynaptic protein synapsin 1 in
350 dissected V1 from *Wld^S* and control C57Bl/6Ola/hsd mice at p20. We found no differences in
351 synapsin 1 levels between these mice (Fig. 4a). To also have a functional readout of excitatory
352 synapse development, we measured the amplitude and interevent intervals of miniature
353 excitatory postsynaptic currents (mEPSC) in pyramidal neurons in layers 2/3 of V1 in *Wld^S* and
354 wildtype mice of p13-14 and p24-25. We found no differences in mEPSC amplitudes or
355 interevent intervals between *Wld^S* and wildtype mice (Fig. 4b, c). Thus, more rapid excitatory
356 synapse development also does not seem to explain the reduced OD plasticity in P28-P35 *Wld^S*
357 mice.

358 **NMNAT3- but not NMNAT1 overexpression reduces OD plasticity**

359 In *Wld^S* mice, a UBE4b-NMNAT1 fusion protein is overexpressed. The effect that this protein
360 has on slowing down Wallerian degeneration depends on its presence in axons (Conforti et al.,
361 2007). However, the *Wld^S* fusion protein is also present in the nucleus. Endogenous NMNAT1 is
362 a nuclear NAD⁺ synthase and is involved in transcriptional regulation (Chang et al., 2010;
363 Pollak et al., 2007). It is thus conceivable that the plasticity changes we observe in *Wld^S* mice
364 are not caused through the signaling pathway that regulates Wallerian degeneration, but
365 through nuclear NMNAT activity.

366 To test this possibility, we examined whether OD plasticity was reduced in a transgenic mouse
367 line overexpressing nuclear NMNAT1 (Yahata et al., 2009). Again, we used optical imaging of
368 intrinsic signal to determine OD in NMNAT1 transgenic mice and wildtype littermates that were
369 either reared normally, or monocular deprived for 7 days (P28-P35). We found that OD plasticity
370 occurred normally in NMNAT1-overexpressing mice (Fig. 5a, b), suggesting that the *Wld^S*
371 mutation does not cause accelerated cortical development by directly altering transcriptional
372 control.

373 To test the alternative hypothesis that increased cytoplasmic NMNAT activity is responsible for
374 decreased OD plasticity towards the end of the critical period, we made use of mice
375 overexpressing NMNAT3. Previous work has shown that in contrast to NMNAT1,
376 overexpression of NMNAT3 slows down Wallerian degeneration, possibly by substituting for
377 cytoplasmic NMNAT2 when it is down-regulated (Avery et al., 2009; Yahata et al., 2009). We
378 found that in NMNAT3-overexpressing mice, OD plasticity after 7 days of MD was significantly
379 reduced (Fig. 5c, d), mimicking the phenotype of *Wld^S* mice. This indicates that the effects
380 observed in *Wld^S* mice are caused by cytoplasmic effects of the UBE4b-NMNAT1 fusion protein
381 rather than by its nuclear activity. These results suggest that the reduction of OD plasticity in
382 *Wld^S* mice during the last week of the critical period probably involves a signaling cascade that
383 involves genes that regulate Wallerian degeneration.

384 **Monocular deprivation does not affect expression of Wallerian-degeneration-related** 385 **proteins**

386 So far, our results show that the signalling pathway that regulates Wallerian degeneration also
387 causes the decline of OD plasticity to occur prematurely in V1. This could imply that OD
388 plasticity actually involves Wallerian degeneration. Alternatively, Wallerian degeneration and
389 cellular events underlying OD plasticity, such as axon growth and retraction and synapse
390 turnover, utilize partially overlapping signalling cascades. To differentiate between these
391 possibilities, we looked for direct signs of Wallerian degeneration during the induction of OD
392 plasticity, such as the presence of activated microglia, or acute regulation of MYCBP2 or
393 NMNAT2 protein levels (Babetto et al., 2013). To determine changes in the levels of MYCBP2
394 and NMNAT2 after MD, we performed quantitative western blot analysis on V1 dissected from
395 the contralateral hemisphere of mice that were monocularly deprived for 7 days and undeprived
396 littermates. No differences in NMNAT2 or MYCBP2 levels were found between tissue from non-
397 deprived and deprived mice (Fig. 6a, b). This suggests that OD plasticity does not involve
398 Wallerian degeneration initiated by MYCBP2/NMNAT2-regulation. We also assessed whether
399 OD plasticity resulted in the presence of activated microglia, a hallmark of Wallerian
400 degeneration. We performed immunohistochemistry with the activated-microglia-specific
401 antibody F4/80 (Castaño et al., 1996) on sections of V1 of C57Bl/6Ola/hsd mice that had been
402 subjected to 7 days of monocular deprivation and undeprived littermates. Assessment of F4/80
403 stained V1 sections did not reveal a significant increase in active microglia between non-
404 deprived and deprived mice (Fig. 6c, d). Thus, we did not find evidence for Wallerian
405 degeneration occurring during OD plasticity, despite the finding that both events are regulated
406 by NMNAT proteins.

407

408 Discussion

409 In this study, we show for the first time that genes known for regulating Wallerian degeneration
410 also control experience-dependent plasticity during development. We demonstrate that
411 compared to control mice, OD plasticity is lower towards the end of the critical period in *Wld^S*
412 mice and visual acuity increases at an earlier age. Interestingly, we did not find any signs of
413 Wallerian degeneration during OD plasticity, suggesting that these processes share a common
414 signalling pathway but do not necessarily involve the same cellular mechanisms of axon
415 degeneration.

416 The *Wld^S* UBE4b-NMNAT1 fusion protein slows down Wallerian degeneration by mislocalizing
417 NMNAT1 to the cytoplasm (Conforti et al., 2007; Sasaki et al., 2016), where it prevents SARM1-
418 dependent NAD⁺ depletion that drives axonal disintegration (Sasaki et al., 2016). Endogenous
419 NMNAT1 is expressed in the nucleus however, where it controls NAD⁺ synthesis and
420 modulates gene transcription (Chang et al., 2010). Our experiments confirm that increased
421 cytoplasmic NMNAT levels also interfere with OD plasticity: in mice overexpressing nuclear
422 NMNAT1, OD plasticity was unaffected while it was reduced in mice overexpressing NMNAT3
423 which localizes to mitochondria and also reduces Wallerian degeneration (Avery et al., 2009;
424 Yahata et al., 2009). Whether increased cytoplasmic NMNAT reduces OD plasticity through
425 preventing SARM1-dependent NAD⁺ depletion or through a different signaling cascade remains
426 to be tested.

427 An earlier study had revealed that axon pruning during development is not altered in *Wld^S* mice
428 or flies expressing the *Wld^S* protein (Hoopfer et al., 2006). This implies that the Wallerian
429 degeneration pathway is only active during pathological axon retraction and does not regulate
430 physiological axon retraction during development. The fact that OD plasticity is affected in *Wld^S*
431 mice and mice overexpressing NMNAT3 shows that the situation is more complex and that
432 during a later phase of cortical development the Wallerian degeneration signalling pathway does
433 have a role in a physiological developmental process. We were not able to determine whether
434 the reduced OD plasticity at the end of the critical period was due to a deficit in axon pruning.
435 We did not find any direct evidence for Wallerian degeneration during OD plasticity in V1, such
436 as altered NMNAT2 or MYCBP2 expression (Gilley and Coleman, 2010) or obvious changes in
437 microglia activation. However, it is possible that OD plasticity does not involve the synchronous
438 retraction of a sufficiently large population of cortical axons to cause detectable changes in
439 these markers. Alternatively, NMNAT proteins may not be involved in acute axonal
440 destabilization during OD plasticity, but regulate cortical plasticity by gradually increasing overall
441 axon or synapse stability in the maturing visual cortex.

442 We found no evidence for activation of microglia after MD. This is in line with a previous study
443 that showed that microglia cells contribute to OD plasticity but did not become activated
444 (Tremblay et al., 2010). However, in this study more subtle changes in microglia morphology
445 and dynamics were observed by *in vivo* two-photon microscopy after brief MD that were
446 essential for effective OD plasticity (Tremblay et al., 2010). Thus, in contrast to the full microglia
447 activation and degeneration of entire axons in Wallerian degeneration after cortical damage, OD
448 plasticity seems to result in a more subtle process involving partial activation of microglia and
449 limited retraction of axonal branches.

450 An early decline of OD plasticity has been observed previously in mice overexpressing BDNF
451 (Hanover et al., 1999; Huang et al., 1999). In these mice, the increase in visual acuity that
452 usually occurs between P25 and P35 also happened at an earlier age, as did the maturation of
453 inhibitory innervation. It is thus possible that also in Wld^S mice, the visual cortex matures faster.
454 We did indeed observe that cortical visual acuity was higher at P25 in Wld^S mice than in control
455 mice. However, we did not observe a more rapid development of cortical inhibitory innervation in
456 Wld^S mice. We also did not find evidence for accelerated excitatory synapse development.
457 Possibly, more subtle developmental alterations of the visual system underlie the rapid increase
458 in visual acuity in Wld^S mice, such as changes in cortical AMPA/NMDA receptor ratios
459 (Saiepour et al., 2017) or thalamic wiring (Stephany et al., 2018). Future studies will have to
460 reveal whether earlier events in visual cortical development, such as transitions in spontaneous
461 activity patterns (Siegel et al., 2012), binocular orientation matching (Wang et al., 2010) or
462 critical period onset (Hensch et al., 1998), also occur at an earlier age in Wld^S mice.

463 In conclusion, this study provides the first evidence that genes in the signaling pathway
464 regulating Wallerian degeneration are also involved in the control of experience-dependent
465 plasticity during normal cortical development. This knowledge may help to reveal the
466 mechanisms involved in critical period closure during cortical development and advance the
467 discovery of novel drug targets for enhancing brain plasticity for therapeutic purposes.

468 **References**

- 469 Antonini a, Fagiolini M, Stryker MP (1999) Anatomical correlates of functional plasticity in
470 mouse visual cortex. *J Neurosci* 19:4388–406.
- 471 Araki T, Sasaki Y, Milbrandt J (2004) Increased nuclear NAD biosynthesis and SIRT1 activation
472 prevent axonal degeneration. *Science* (80-) 305:1010–1013.
- 473 Avery MA, Sheehan AE, Kerr KS, Wang J, Freeman MR (2009) Wld s requires Nmnat1
474 enzymatic activity and N16- VCP interactions to suppress Wallerian degeneration. *J Cell*
475 *Biol* 184:501–513.
- 476 Babetto E, Beirowski B, Russler E, Milbrandt J, DiAntonio A (2013) The Phr1 Ubiquitin Ligase
477 Promotes Injury-Induced Axon Self-Destruction. *Cell Rep* 3:1422–1429.
- 478 Bear MF, Singer W (1986) Modulation of visual cortical plasticity by acetylcholine and
479 noradrenaline. *Nature* 320:172–176.
- 480 Bochner DN, Sapp RW, Adelson JD, Zhang S, Lee H, Djuricic M, Syken J, Dan Y, Shatz CJ
481 (2014) Blocking PirB up-regulates spines and functional synapses to unlock visual cortical
482 plasticity and facilitate recovery from amblyopia. *Sci Transl Med* 6:258ra140.
- 483 Castaño A, Lawson LJ, Fearn S, Perry VH (1996) Activation and proliferation of murine
484 microglia are insensitive to glucocorticoids in Wallerian degeneration. *Eur J Neurosci*
485 8:581–8.
- 486 Chang J, Zhang B, Heath H, Galjart N, Wang X, Milbrandt J (2010) Nicotinamide adenine
487 dinucleotide (NAD)-regulated DNA methylation alters CCCTC-binding factor
488 (CTCF)/cohesin binding and transcription at the BDNF locus. *Proc Natl Acad Sci*
489 107:21836–21841.
- 490 Chattopadhyaya B (2004) Experience and Activity-Dependent Maturation of Perisomatic
491 GABAergic Innervation in Primary Visual Cortex during a Postnatal Critical Period. *J*
492 *Neurosci* 24:9598–9611.
- 493 Coleman MP, Conforti L, Buckmaster EA, Tarlton A, Ewing RM, Brown MC, Lyon MF, Perry VH
494 (1998) An 85-kb tandem triplication in the slow Wallerian degeneration (Wlds) mouse. *Proc*
495 *Natl Acad Sci U S A* 95:9985–90.
- 496 Coleman MP, Freeman MR (2010) Wallerian degeneration, wld(s), and nmnat. *Annu Rev*
497 *Neurosci* 33:245–267.
- 498 Conforti L, Fang G, Beirowski B, Wang MS, Sorci L, Asress S, Adalbert R, Silva a, Bridge K,
499 Huang XP, Magni G, Glass JD, Coleman MP (2007) NAD(+) and axon degeneration
500 revisited: Nmnat1 cannot substitute for Wld(S) to delay Wallerian degeneration. *Cell Death*
501 *Differ* 14:116–127.
- 502 Conforti L, Tarlton A, Mack TG, Mi W, Buckmaster EA, Wagner D, Perry VH, Coleman MP
503 (2000) A Ufd2/D4Cole1e chimeric protein and overexpression of Rbp7 in the slow
504 Wallerian degeneration (WldS) mouse. *Proc Natl Acad Sci U S A* 97:11377–11382.
- 505 Conforti L, Wilbrey A, Morreale G, Janeckova L, Beirowski B, Adalbert R, Mazzola F, Stefano M
506 Di, Hartley R, Babetto E, Smith T, Gilley J, Billington RA, Genazzani AA, Ribchester RR,
507 Magni G, Coleman M (2009) Wld S protein requires Nmnat activity and a short N-terminal
508 sequence to protect axons in mice. *J Cell Biol* 184:491–500.

- 509 Dahlhaus M, Wan Li K, van der Schors RC, Saiepour MH, van Nierop P, Heimel JA, Hermans
510 JM, Loos M, Smit AB, Levelt CN (2011) The Synaptic Proteome during Development and
511 Plasticity of the Mouse Visual Cortex. *Mol Cell Proteomics* 10:M110.005413.
- 512 del Rio JA, de Leca (1994) The development of parvalbumin immunoactivity in the neocortex of
513 the mouse. *Science* (80-) 5:247–259.
- 514 Fagiolini M (2004) Specific GABAA Circuits for Visual Cortical Plasticity. *Science* (80-)
515 303:1681–1683.
- 516 Geden MJ, Deshmukh M (2016) Axon degeneration: Context defines distinct pathways. *Curr*
517 *Opin Neurobiol*.
- 518 Gerdtz J, Summers DW, Milbrandt J, DiAntonio A (2016) Axon Self-Destruction: New Links
519 among SARM1, MAPKs, and NAD+ Metabolism. *Neuron*.
- 520 Gianfranceschi L, Siciliano R, Walls J, Morales B, Kirkwood A, Huang ZJ, Tonegawa S, Maffei L
521 (2003) Visual cortex is rescued from the effects of dark rearing by overexpression of
522 BDNF. *Proc Natl Acad Sci* 100:12486–12491.
- 523 Gilley J, Coleman MP (2010) Endogenous Nmnat2 Is an Essential Survival Factor for
524 Maintenance of Healthy Axons. *PLoS Biol* 8.
- 525 Gordon A, Stryker P (1996) Experience-Dependent Plasticity of Binocular Responses in the
526 Primary Visual Cortex of the Mouse. *J Neurosci* 16:3274–3286.
- 527 Hanover JL, Huang ZJ, Tonegawa S, Stryker MP (1999) Brain-derived neurotrophic factor
528 overexpression induces precocious critical period in mouse visual cortex. *J Neurosci*
529 19:RC40.
- 530 Haruta M, Hata Y (2007) Experience-Driven Axon Retraction without Binocular Imbalance in
531 Developing Visual Cortex. *Curr Biol* 17:37–42.
- 532 Heimel JA, Hartman RJ, Hermans JM, Levelt CN (2007) Screening mouse vision with intrinsic
533 signal optical imaging. *Eur J Neurosci* 25:795–804.
- 534 Hensch TK (2005) Critical period plasticity in local cortical circuits. *Nat Rev Neurosci* 6:877–888.
- 535 Hensch TK, Fagiolini M, Mataga N, Stryker MP, Baekkeskov S, Kash SF (1998) Local GABA
536 circuit control of experience-dependent plasticity in developing visual cortex. *Science*
537 282:1504–8.
- 538 Hofer SB, Mrcic-Flogel TD, Bonhoeffer T, Hübener M (2006) Lifelong learning: ocular
539 dominance plasticity in mouse visual cortex. *Curr Opin Neurobiol* 16:451–459.
- 540 Hoopfer ED, McLaughlin T, Watts RJ, Schuldiner O, O’Leary DDM, Luo L (2006) Wlds
541 Protection Distinguishes Axon Degeneration following Injury from Naturally Occurring
542 Developmental Pruning. *Neuron* 50:883–895.
- 543 Huang X, Stodieck SK, Goetze B, Cui L, Wong MH, Wenzel C, Hosang L, Dong Y, Löwel S,
544 Schlüter OM (2015) Progressive maturation of silent synapses governs the duration of a
545 critical period. *Proc Natl Acad Sci* 112:E3131–E3140.
- 546 Huang ZJ, Kirkwood A, Pizzorusso T, Porciatti V, Morales B, Bear MF, Maffei L, Tonegawa S
547 (1999) BDNF regulates the maturation of inhibition and the critical period of plasticity in
548 mouse visual cortex. *Cell* 98:739–55.

- 549 Jenks KR, Kim T, Pastuzyn ED, Okuno H, Taibi A V., Bito H, Bear MF, Shepherd JD (2017) Arc
550 restores juvenile plasticity in adult mouse visual cortex. *Proc Natl Acad Sci*
551 114:201700866.
- 552 Kerschensteiner M, Schwab ME, Lichtman JW, Misgeld T (2005) In vivo imaging of axonal
553 degeneration and regeneration in the injured spinal cord. *Nat Med* 11:572–577.
- 554 Kuhlman SJ, Olivas ND, Tring E, Ikrar T, Xu X, Trachtenberg JT (2013) A disinhibitory
555 microcircuit initiates critical-period plasticity in the visual cortex. *Nature* 501:543–546.
- 556 Lehmann K, Löwel S (2008) Age-Dependent Ocular Dominance Plasticity in Adult Mice. *PLoS*
557 *One* 3:e3120.
- 558 Levelt CN, Hübener M (2012) Critical-Period Plasticity in the Visual Cortex. *Annu Rev Neurosci*
559 35:309–330.
- 560 Lohmann C, Kessels HW (2014) The developmental stages of synaptic plasticity. *J Physiol*
561 592:13–31.
- 562 Lunn ER, Perry VH, Brown MC, Rosen H, Gordon S (1989) Absence of Wallerian Degeneration
563 does not Hinder Regeneration in Peripheral Nerve. *Eur J Neurosci* 1:27–33.
- 564 Lyon MF, Ogunkolade BW, Brown MC, Atherton DJ, Perry VH (1993) A gene affecting Wallerian
565 nerve degeneration maps distally on mouse chromosome 4. *Proc Natl Acad Sci U S A*
566 90:9717–20.
- 567 McGee AW, Yang Y, Fischer QS, Daw NW, Strittmatter SH (2005) Neuroscience: Experience-
568 driven plasticity of visual cortex limited by myelin and nogo receptor. *Science* (80-)
569 309:2222–2226.
- 570 Morishita H, Hensch TK (2008) Critical period revisited: impact on vision. *Curr Opin Neurobiol*
571 18:101–107.
- 572 Pease SE, Segal RA (2014) Preserve and protect: Maintaining axons within functional circuits.
573 *Trends Neurosci*.
- 574 Pham TA, Graham SJ, Suzuki S, Barco A, Kandel ER, Gordon B, Lickey ME (2004) A semi-
575 persistent adult ocular dominance plasticity in visual cortex is stabilized by activated CREB.
576 *Learn Mem* 11:738–747.
- 577 Pizzorusso T, Medini P, Berardi N, Chierzi S, Fawcett JW, Maffei L (2002) Reactivation of
578 ocular dominance plasticity in the adult visual cortex. *Science* (80-) 298:1248–1251.
- 579 Pollak N, Dölle C, Ziegler M (2007) The power to reduce: pyridine nucleotides – small molecules
580 with a multitude of functions. *Biochem J* 402:205–218.
- 581 Saiepour MH, Min R, Kamphuis W, Heimel JA, Levelt CN (2017) β -Catenin in the Adult Visual
582 Cortex Regulates NMDA-Receptor Function and Visual Responses. *Cereb Cortex*.
- 583 Sasaki Y, Araki T, Milbrandt J (2006) Stimulation of Nicotinamide Adenine Dinucleotide
584 Biosynthetic Pathways Delays Axonal Degeneration after Axotomy. *J Neurosci* 26:8484–
585 8491.
- 586 Sasaki Y, Nakagawa T, Mao X, DiAntonio A, Milbrandt J (2016) NMNAT1 inhibits axon
587 degeneration via blockade of SARM1-mediated NAD⁺ depletion. *Elife* 5.
- 588 Sato M, Stryker MP (2008) Distinctive Features of Adult Ocular Dominance Plasticity. *J*

- 589 Neurosci 28:10278–10286.
- 590 Sawtell NB, Frenkel MY, Philpot BD, Nakazawa K, Tonegawa S, Bear MF (2003) NMDA
591 receptor-dependent ocular dominance plasticity in adult visual cortex. *Neuron* 38:977–985.
- 592 Siegel F, Heimel JA, Peters J, Lohmann C (2012) Peripheral and Central Inputs Shape Network
593 Dynamics in the Developing Visual Cortex In Vivo. *Curr Biol* 22:253–258.
- 594 Sommeijer JP, Levelt CN (2012) Synaptotagmin-2 is a reliable marker for parvalbumin positive
595 inhibitory boutons in the mouse visual cortex. *PLoS One* 7:e35323.
- 596 Stephany C-E, Chan LLH, Parivash SN, Dorton HM, Piechowicz M, Qiu S, McGee AW (2014)
597 Plasticity of Binocularity and Visual Acuity Are Differentially Limited by Nogo Receptor. *J*
598 *Neurosci* 34:11631–11640.
- 599 Stephany C-É, Ma X, Dorton HM, Wu J, Solomon AM, Frantz MG, Qiu S, McGee AW (2018)
600 Distinct Circuits for Recovery of Eye Dominance and Acuity in Murine Amblyopia. *Curr Biol*
601 28:1914–1923.e5.
- 602 Syken J, GrandPre T, Kanold PO, Shatz CJ (2006) PirB restricts ocular-dominance plasticity in
603 visual cortex. *Science* (80-) 313:1795–1800.
- 604 Tognini P, Putignano E, Coatti A, Pizzorusso T (2011) Experience-dependent expression of
605 miR-132 regulates ocular dominance plasticity. *Nat Neurosci* 14:1237–1239.
- 606 Tremblay MĚ, Lowery RL, Majewska AK (2010) Microglial interactions with synapses are
607 modulated by visual experience. *PLoS Biol* 8.
- 608 Tropea D, Majewska AK, Garcia R, Sur M (2010) Structural Dynamics of Synapses in Vivo
609 Correlate with Functional Changes during Experience-Dependent Plasticity in Visual
610 Cortex. *J Neurosci* 30:11086–11095.
- 611 Vargas ME, Barres BA (2007) Why Is Wallerian Degeneration in the CNS So Slow? *Annu Rev*
612 *Neurosci* 30:153–179.
- 613 Vetencourt JFM, Sale A, Viegi A, Baroncelli L, De Pasquale R, F. O'Leary O, Castren E, Maffei
614 L (2008) The Antidepressant Fluoxetine Restores Plasticity in the Adult Visual Cortex.
615 *Science* (80-) 320:385–388.
- 616 Wang B-S, Sarnaik R, Cang J (2010) Critical Period Plasticity Matches Binocular Orientation
617 Preference in the Visual Cortex. *Neuron* 65:246–256.
- 618 Yahata N, Yuasa S, Araki T (2009) Nicotinamide Mononucleotide Adenylyltransferase
619 Expression in Mitochondrial Matrix Delays Wallerian Degeneration. *J Neurosci* 29:6276–
620 6284.
- 621
- 622

623 **Legends**

624 **Figure 1: Wld^S mutant mice have reduced OD plasticity during the critical period.**

625 **a**, Transcranial images of change in light reflection in V1, in response to individual eye
626 stimulation in non-deprived (no MD) and 7 day-deprived (7d MD) wildtype (WT) and Wld^S mice,
627 during the peak of the critical period at postnatal (P) days 28-35. **b**, Imaged Ocular Dominance
628 Index (iODI) shows that 7d MD induces a larger OD shift in wildtype (WT) mice than in Wld^S
629 mutant mice (interaction genotype/OD-shift: two-way Anova, $P=0.0029$, post-hoc Tukey's, WT
630 vs WT MD, $P<0.0001$, Wld^S vs Wld^S MD, $P=0.0114$, WT MD vs Wld^S MD, $P=0.0034$, WT: $n=12$
631 mice, Wld^S : $n=9$ mice, WT MD: $n=8$ mice, Wld^S MD: $n=7$ mice). **c**, Transcranial images of
632 change in light reflection in V1, in response to individual eye stimulation in no MD and 7d MD
633 WT and Wld^S mice, before the peak of the critical period. **d**, Imaged ODIs show that earlier in
634 development MD induces an OD shift in both WT and Wld^S mice, with no significant difference
635 between the genotypes (interaction genotype/OD-shift: two-way Anova, $P=0.4018$; interaction
636 treatment/OD-shift: $P<0.0001$, post-hoc Tukey's, WT vs WT MD, $P=0.0022$, Wld^S vs Wld^S MD,
637 $P=0.0021$. WT: $n=8$ mice, Wld^S : $n=5$ mice, WT MD: $n=6$ mice, Wld^S MD: $n=5$ mice). Values
638 shown as median (solid line), ± 1.5 interquartile range (box) and minimal and maximal values
639 (whiskers). Scale bars, 200 μm . * $P<0.05$, ** $P<0.01$, **** $P<0.0001$.

640 **Figure 2: Early increase of visual acuity in Wld^S mice.**

641 **a**, Transcranial images of light reflection in V1, in response to visual stimulation using sinusoidal
642 gratings with different spatial frequencies. Scale bar, 1 mm. **b**, Example of cortical responses
643 and the inferred acuity of a wildtype (WT) mouse. **c**, Acuity of V1 responses is significantly
644 increased in Wld^S mutant mice compared to WT mice at postnatal (P) day 25 (t-test, $P=0.015$,
645 WT: $n=7$, Wld^S : $n=4$).

646 **Figure 3: Normal development of inhibitory innervation in *Wld^S* mice.**

647 **a**, Representative images showing synaptotagmin 2 (syt 2) positive puncta forming rings
648 around cell bodies in cortical layers 2/3 in wildtype (WT) and *Wld^S* mice at postnatal day (P) 20
649 and 30. Number of syt 2 expressing boutons forming puncta rings in layers 2/3 are unchanged
650 in *Wld^S* mice compared to WT controls at P20 (t-test, $P=0.577$, $n=4$ for both genotypes) or P30
651 ($P=0.521$, $n=5$ for both genotypes). **b**, Representative images showing syt 2 positive puncta
652 forming rings around cell bodies in cortical layer 5 in WT and *Wld^S* mice at P20 and P30.
653 Number of syt 2 expressing boutons forming puncta rings in layer 5 are unchanged in *Wld^S* mice
654 compared to WT controls at P20 (t-test, $P=0.785$, $n=4$ for both genotypes), or P30 ($P=0.461$,
655 $n=5$ for both genotypes). **c**, Representative examples of western blot analysis of V1 and
656 quantification of expression levels, normalized to those of WT control mice. Expression levels
657 for syt 2 are unaltered at P30 (t-test, $P=0.9869$, $n=6$ for both genotypes) **d**, *GAD65* mRNA
658 expression levels relative to housekeeping gene is unchanged at P30 ($P=0.089$, WT: $n=8$, *Wld^S*:
659 $n=7$). Values shown as median (solid line), ± 1.5 interquartile range (box) and minimal and
660 maximal values (whiskers). Scale bars, 10 μm .

661 **Figure 4: Unaltered cortical excitation in Wld^S mutant mice.**

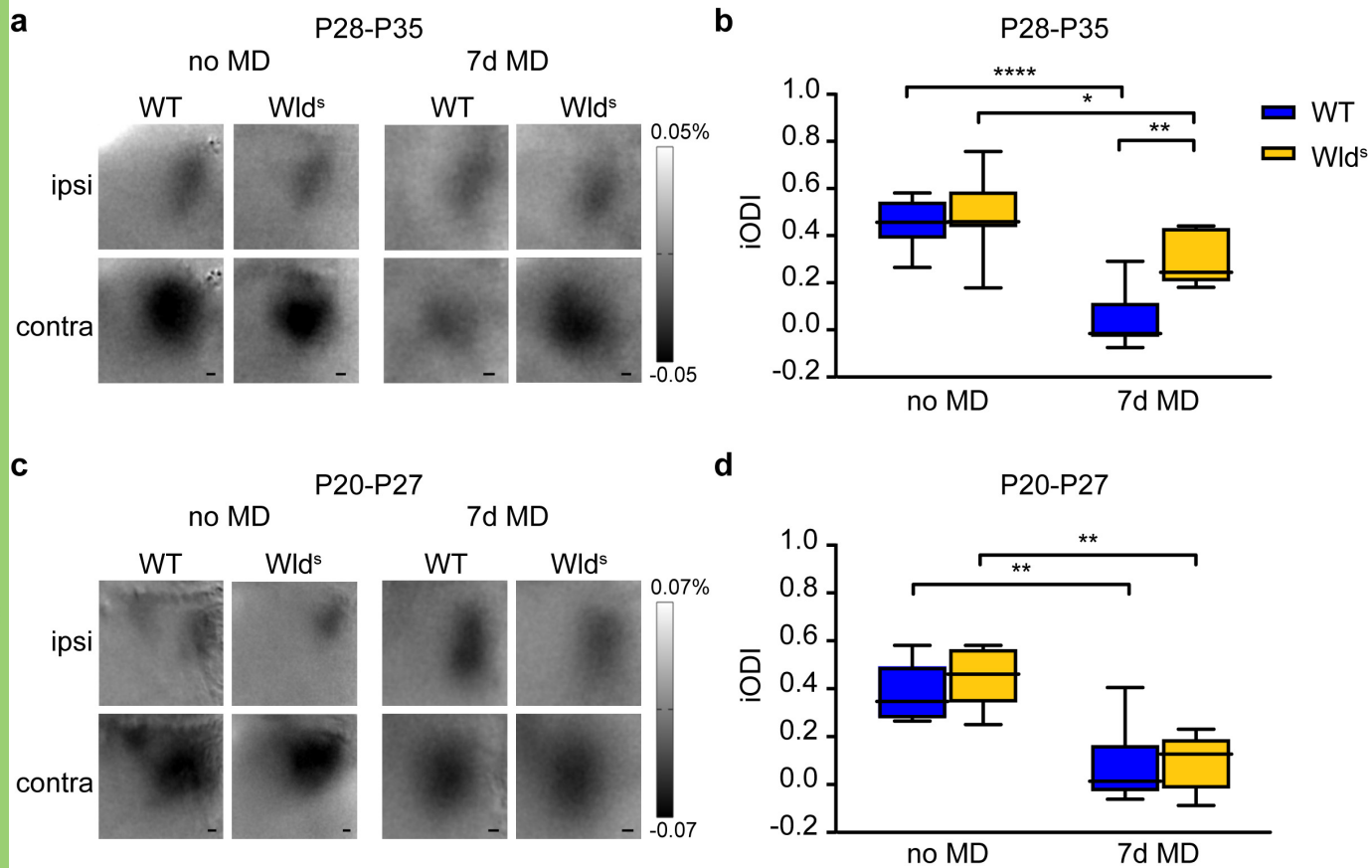
662 **a**, Representative examples of western blot analysis of V1 and quantification of expression
663 levels, normalized to those of wildtype (WT) control mice. Expression levels for synapsin 1 are
664 unaltered at postnatal day (P) 20 (t-test, $P=0.5091$, $n=6$ for both genotypes). Values shown as
665 median (solid line), ± 1.5 interquartile range (box) and minimal and maximal values (whiskers).
666 **b-c**, Cumulative distributions of the amplitude (**b**) or inter event interval (**c**) of mEPSC in Wld^S
667 (yellow) or WT (blue) mice at P13-14 (solid line) or P24-25 (dotted line). Excitatory input to
668 pyramidal neurons shows no significant change in amplitude between Wld^S and WT control
669 mice at P13-14 (t-test, $P=0.55$, WT: $n=10$, Wld^S : $n=5$) or P24-25 ($P=0.59$, WT: $n=9$, Wld^S : $n=13$).
670 Frequencies of mEPSCs in Wld^S mice and WT controls also show no significant difference
671 between the two genotypes (P13-14: $P = 0.84$, P24-25: $P=0.23$, n =same is as in **a**).

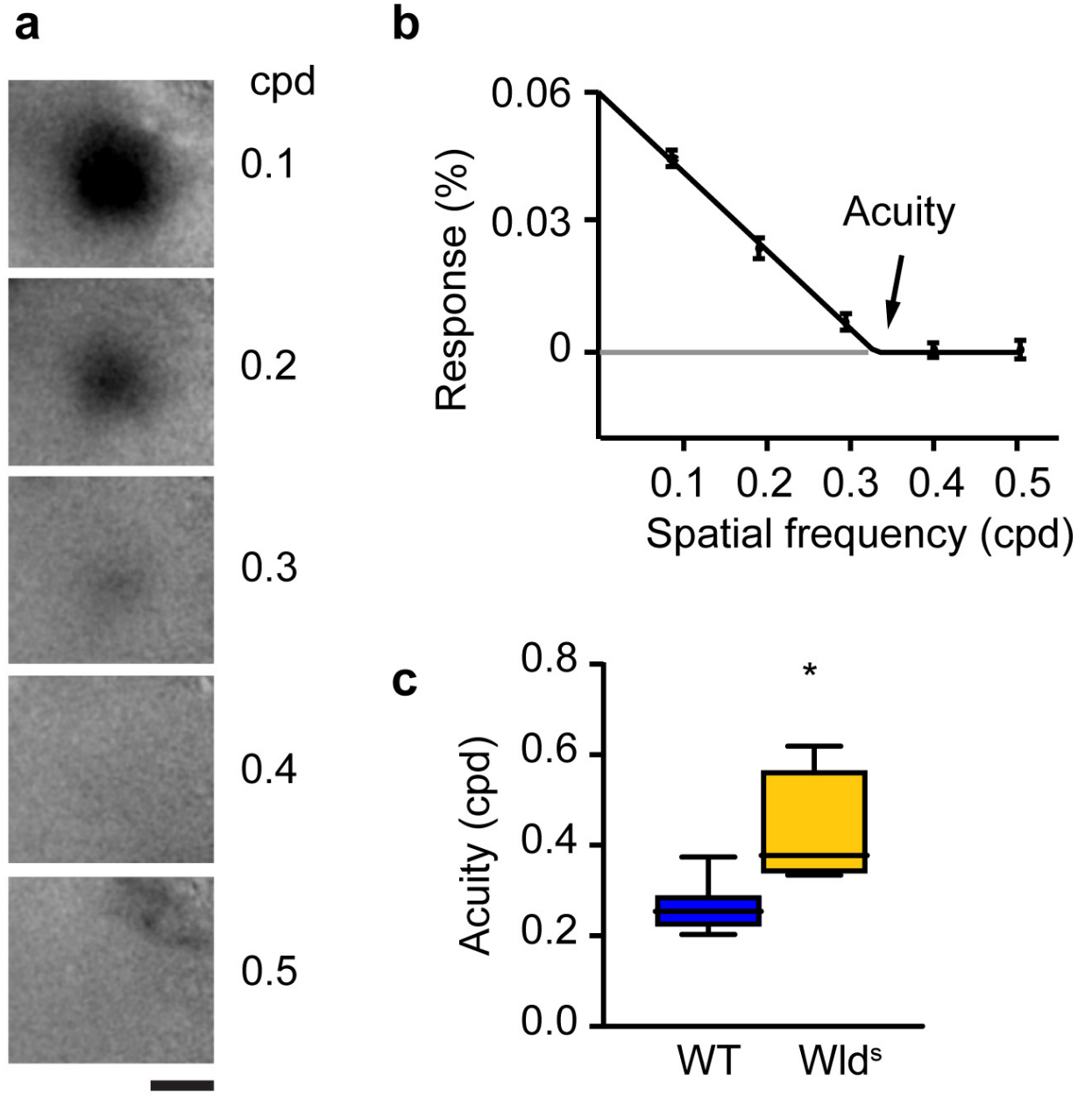
672 **Figure 5: NMNAT3- but not NMNAT1 overexpression reduces OD plasticity.**

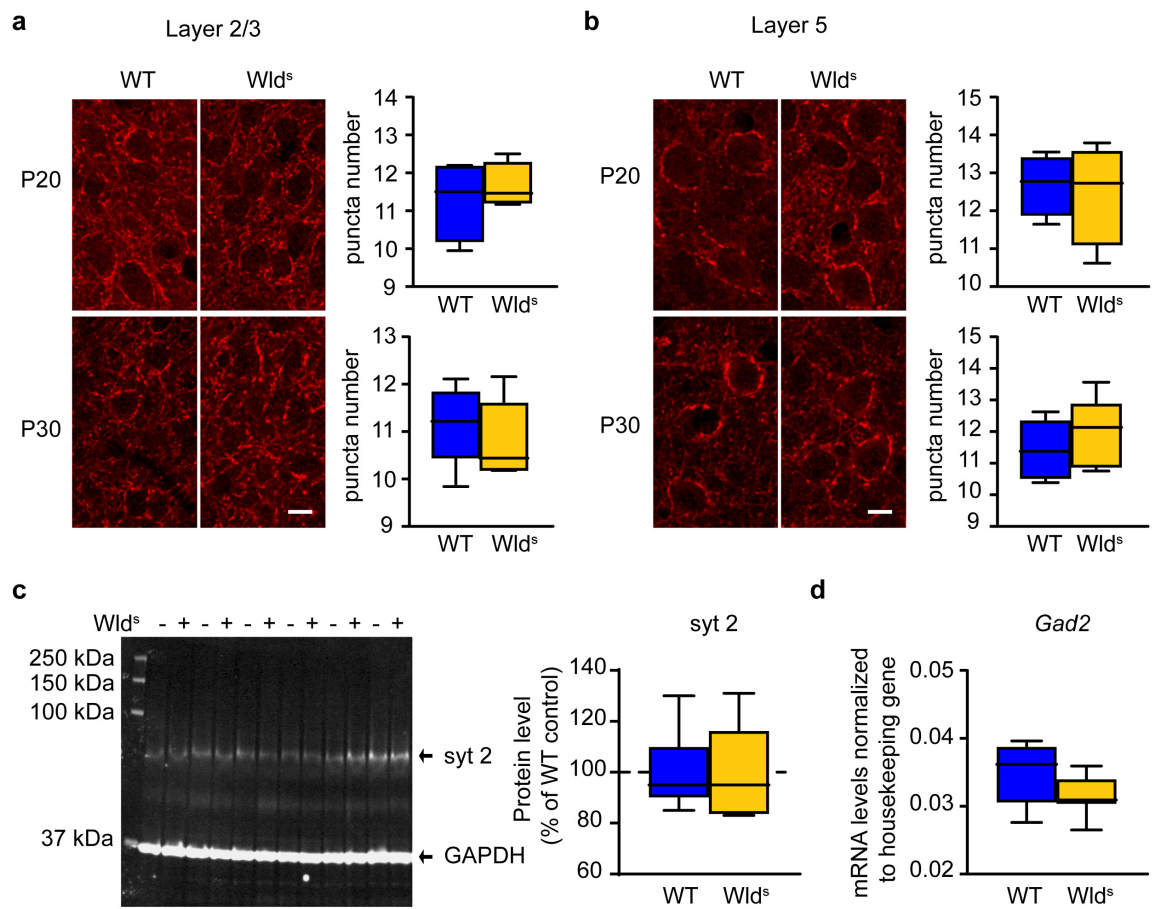
673 **a**, Transcranial images of change in light reflection in V1, in response to individual eye
674 stimulation in non-deprived (no MD) and 7 day-deprived (7d MD) wildtype (WT) and NMNAT1
675 mice. **b**, Imaged Ocular Dominance Index (iODI) shows that 7d MD during the peak of the
676 critical period induces an OD shift both in WT mice and in NMNAT1 mice (interaction
677 genotype/OD-shift: two-way Anova, $P=0.235$; interaction treatment/OD-shift: $P<0.0001$, post-
678 hoc Tukey's, WT vs WT MD, $P=0.0033$, NMNAT1 vs NMNAT1 MD, $P=0.0015$. WT: $n=3$ mice,
679 NMNAT1: $n=3$, WT MD: $n=4$, NMNAT1 MD: $n=5$). **c**, Transcranial images of change in light
680 reflection in V1, in response to individual eye stimulation in no MD and 7d MD WT and NMNAT3
681 mice. **d**, Imaged ODIs show that 7d MD during the peak of the critical period, induces a larger
682 OD shift in WT mice than in NMNAT3 mice (interaction genotype/OD-shift: two-way Anova,
683 $P=0.0475$; interaction treatment/OD-shift: $P<0.0001$, post-hoc Tukey's, WT vs WT MD,
684 $P=0.001$, WT MD vs NMNAT3 MD, $P=0.0283$, NMNAT3 vs NMNAT3 MD, $P=0.09$. WT: $n=7$,
685 NMNAT3: $n=8$, WT MD: $n=11$, Wild^S MD: $n=16$). Values shown as median (solid line), ± 1.5
686 interquartile range (box) and minimal and maximal values (whiskers). * $P<0.05$, ** $P<0.01$.

687 **Figure 6: Monocular deprivation does not affect expression of Wallerian-degeneration-**
688 **related proteins.**

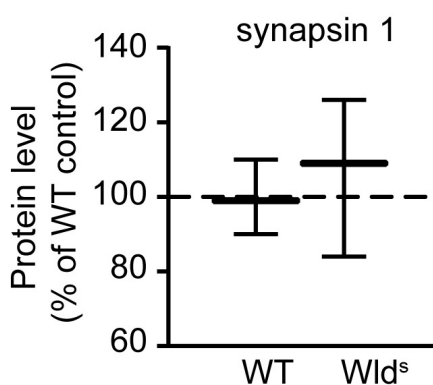
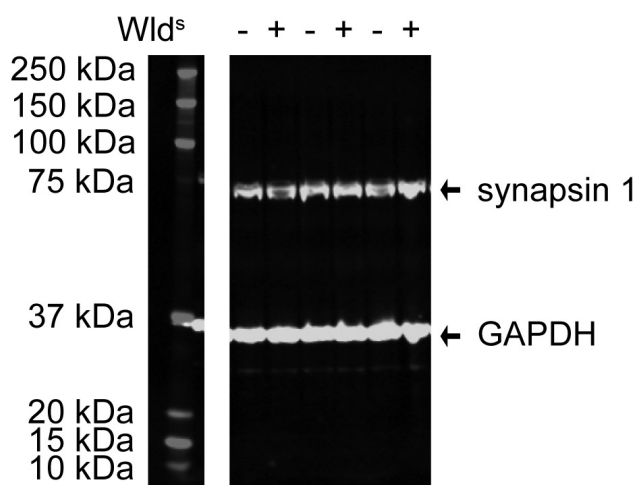
689 **a**, Representative examples of western blot analysis of V1 homogenates of wildtype (WT) mice
690 at postnatal day 37 with (+) or without (-) 7 days monocular deprivation (MD) for MYCBP2 and
691 NMNAT2 expression. **b**, Quantification of expression levels, normalized to those of non-
692 deprived WT control mice. Expression levels for both MYCBP2 and NMNAT2 are unaltered in
693 V1 after MD (t-test, MYCBP2: $P=0.992$, both conditions: $n=6$; NMNAT2: $P=0.985$, no MD: $n=7$,
694 MD: $n=6$). **c**, Examples and quantification of F4/80 stainings for activated microglia in WT
695 control mice with or without 7 days MD. The number of activated microglia per $387.5 \mu\text{m} \times$
696 $387.5 \mu\text{m}$ area of V1 is not significantly different with or without 7 days MD (t-test, $P=0.821$, no
697 MD: $n=4$ mice; MD: $n=3$ mice). Values shown as median (solid line), ± 1.5 interquartile range
698 (box) and minimal and maximal values (whiskers). Scale bars, $50 \mu\text{m}$



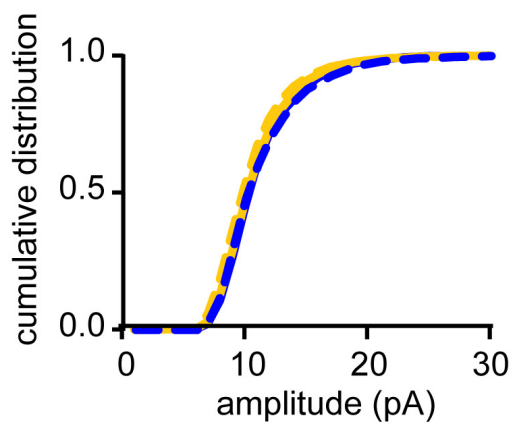




a



b



c

